THE MECHANICAL DESIGN OF A MODULAR DIRECT CONNECT TEST ARTICLE

C.R. Starace and C.J. Smith
North Wind
Ronkonkoma, New York

M.D. Bynum
NASA Langley Research Center
Hampton, VA

ABSTRACT

Currently, experimental data for the design of cavity flameholders of dual-mode ramjets at combustor flameout is limited. As high-speed airbreathing flight becomes more prevalent, this narrow scope of data could result in performance benefits being left unrecognized. To explore the impact of cavity geometry on dual-mode ramjet combustor operability, the NASA Langley Research Center (LaRC) has contracted North Wind to design two test articles to support the Technical Challenge 3 (TC-3) research program. The plan is to conduct these tests in NASA LaRC's Direct-Connect Supersonic Combustion Test Facility (DCSCTF). These two test articles, one photoscaled to be half the size of the other, are being designed with modular cavities, fuel injector blocks, and window stations to allow NASA to test combustor performance across a wide variety of geometries and conditions. Each test article also includes an actuated choke device to provide backpressure in cases when fuel is not injected into the core flow. To allow for operation at conditions equivalent to flight enthalpies from Mach 5 to Mach 7, three different copper types, C10100, C18150, and GRCop-42, were selected for most components. Yttria Stabilized Zirconia (7YSZ) is being used as a thermal barrier coating and additive manufacturing allows for the routing of complex fuel and coolant passages used to ensure survivability. Thermal-structural analysis was conducted using ANSYS to validate and optimize the mechanical design of the test articles. This paper summarizes the state of the design and analysis of the TC-3 test articles up to the Critical Design Review (CDR).

INTRODUCTION

The Technical Challenge 3 (TC-3) project began in 2022 by NASA's High-Speed Flight Project (HSF) with the aim of developing improved scaling laws for cavities in high-speed combustors. The cavity is used to aid the mixing of fuel and air to improve combustion but also increase the drag of the engine as well as its weight due to measures required to deal with increased heat loads in the cavity. If the cavity can be reduced in size without a corresponding loss in combustion efficiency, the overall performance of a dual-mode ramjet-powered vehicle can be improved. The TC-3 challenge statement is: To improve current engine (1X) performance and enable engine scale-up to fully reusable vehicle scales (100X). NASA will develop and deliver mathematical models and associated validation test data with quantified uncertainty that support the design of high-speed combustors inclusive of next generation synthetic fuels. NASA will demonstrate such capability by reducing the length of the state-of-the-art cavity flameholder by 25%. The combustor selected for this 25% cavity flameholder length demonstration is the HIFiRE Direct Connect Rig (HDCR) [1].

To achieve these research objectives, TC-3 will use two modular test articles built around a photoscaled flowpath. The smaller "0.5X Scale" article is half the size of the larger "2X Scale" article, with 25% of the mass flow. Each test article will be able to support nine cavity geometries of varying depths (0.50 inches, 1.00 inch, and 2.00 inches for the larger test article and 0.25 inches, 0.50 inches, and 1.00 inch on the smaller one) and lengths (3, 5, and 7 L/D for both test articles). In addition, there are two modular upstream fuel injector blocks (FIBs) featuring a set of struts and ramps with injector ports. These will have constant geometry while supporting different types of fuel. TC-3 intends to investigate the performance of five fuels: Three gases (hydrogen, ethylene, and a 64-36 mixture of ethylene and

.

methane) and two liquids (JP-10 and a synthetically derived aviation fuel based on camelina oil). A variety of sensors will be used to observe combustion in the test article, including static pressure taps, high-frequency pressure transducers, thermocouples, heat flux gauges, fuel-air equivalence ratio sensors, and optical and infrared cameras. Figure 1 shows a set of propulsion keel lines for the combustor showing the nine cavity configurations in each test article, while Figure 2 shows the various fuel injection sites with the "intended fueling areas" shown using simple geometric shapes.

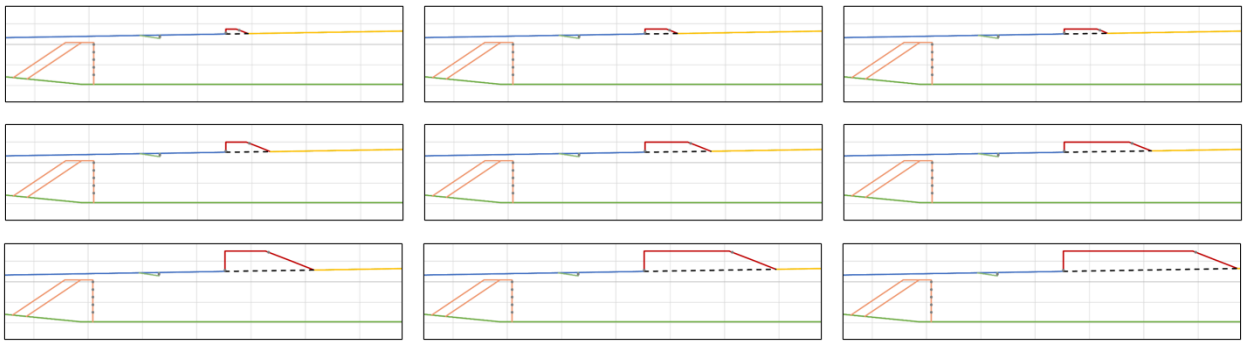


Figure 1: Propulsion keel lines of the combustor region. The protrusions for the FIBs may be seen at the upstream (left) side of each diagram, while the various cavity geometries are shown on the downstream (right) side.

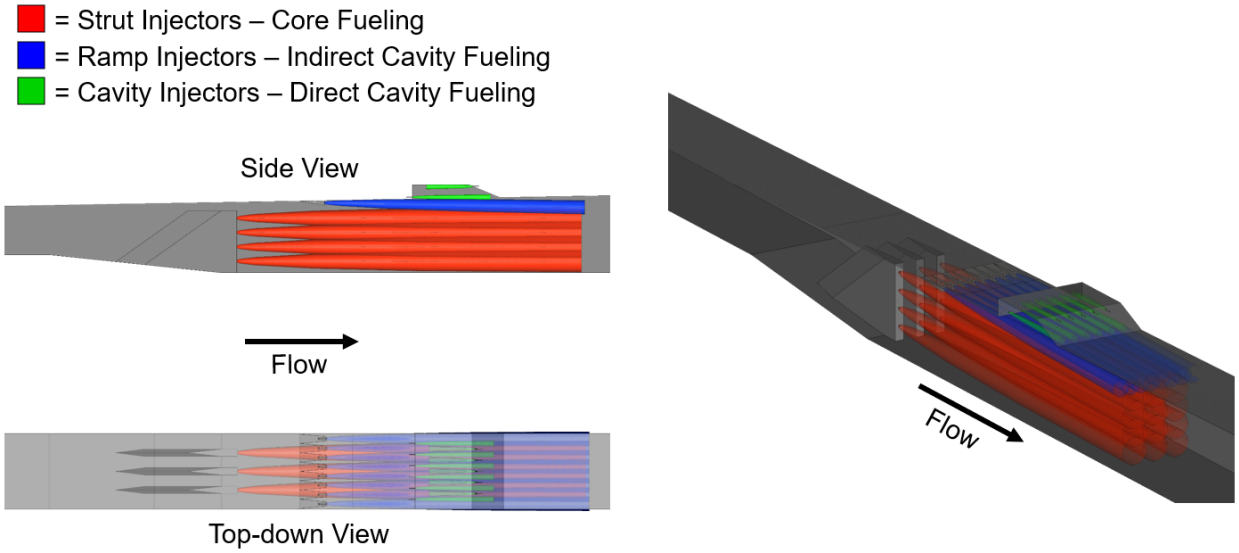


Figure 2: Side, Top-down, and isometric views of the fuel injectors and their intended fueling areas in each test article. Note that not all fuel injectors will be run in each test.

Initial estimates for performance will be made based on CFD (RANS and LES). These will be compared to results from three different types of experiments. The first, a non-burning mixing test, will investigate how well the various cavity geometries mix fuel from the Ramp Fuel Injector Block (FIB). This experiment will use a single gaseous fuel and will be run at the lower-enthalpy condition for each of the two facility nozzles used by each test article (Mach 5 and Mach 6, for the facility Mach 2.1 and Mach 2.65 nozzles respectively). Next, a series of cavity-only combustion tests will be conducted for all five fuel types to determine which cavity geometry produces the most "robust" combustion, with "robustness" being how well the cavity sustains combustion over a range of equivalence ratios. Finally, the core-flow reaction test will use fuel injection from all injector sites to determine which cavity is best at maintaining core flow combustion. The latter two tests will cover each permutation of cavity size, fuel type, flight enthalpy, nozzle, and dynamic pressure (750 psf and 1,500 psf conditions will be investigated). Particular

attention will be paid to the minimum fuel flow required to maintain combustion. Figure 3 shows CFD analysis that was used as a surrogate for a sample ground test case showing flameout occurring solely by varying the fueling in the cavity and core flow.

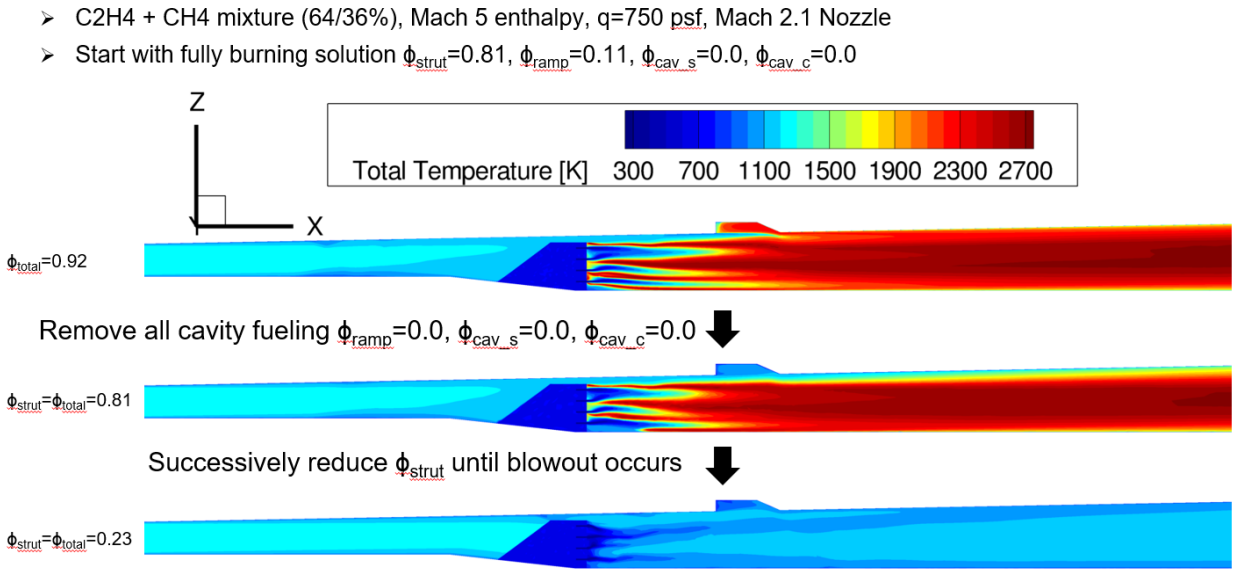


Figure 3: A sample TC-3 test run with fuel flow being drawn down after ignition. The run shown is for a core flow mixing experiment.

This paper focuses on the mechanical design and supporting analysis of the two test articles for TC-3.

DESCRIPTION OF TEST ARTICLE DESIGN

OVERVIEW

Each test article contains a 2D flowpath and is divided into three subassemblies for ease of manufacturing and assembly. They include the isolator, the combustor, and the nozzle. All three are of simple box construction with sidewalls bolted to the body- and cowl-side walls, which are then bolted together in turn to produce the flowpath. The isolator has a bolted interface to the facility nozzle at its upstream end. The 2X scale version interfaces with a pair of preexisting DCSCTF facility nozzles while the 0.5X scale version connects to a pair of new-build facility nozzles based on the existing nozzle designs. The combustor subassemblies contain all the modular components as well as all of the windows. Finally, the test article nozzles contain the sole actuated component in the form of a back pressure device. The gap between the trailing end of the test article is bridged by a simple ejector transition duct of welded steel construction. Overall length of the 2X scale version is 110 in with a span of 5.603 in, while the smaller 0.5X version is 55 in and 2.304 in, respectively. The flowpath of the 0.5X scale test article is photoscaled from the larger one, though this does not extend to the outer mold line. All-up weight is approximately 2,900 lbs for the 2X test articles and 760 lbs for the 0.5X scale. Section views of each test article may be seen in Figures 4 and 5.

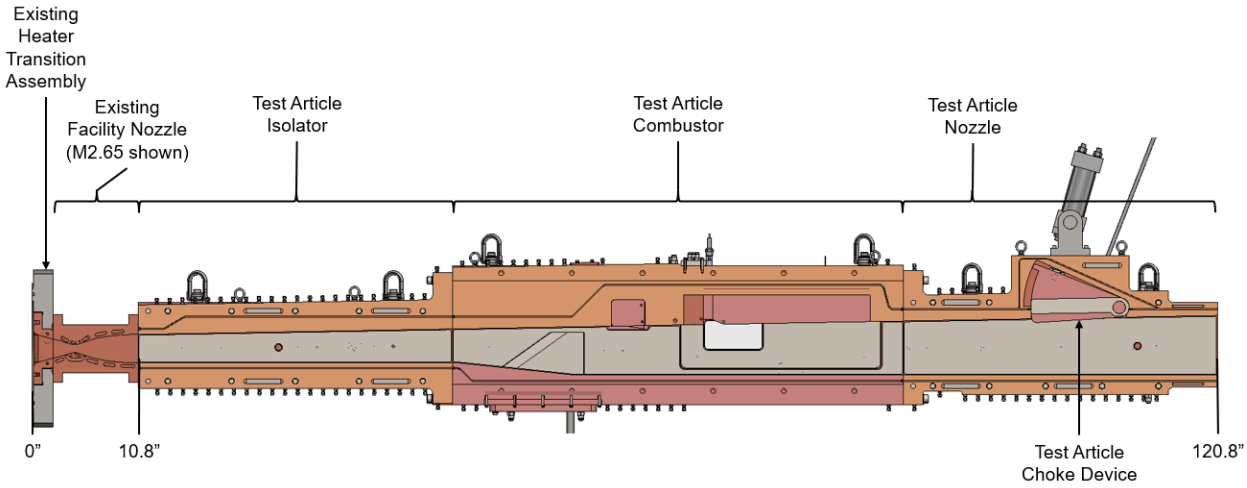


Figure 4: 2X scale test article with facility nozzle

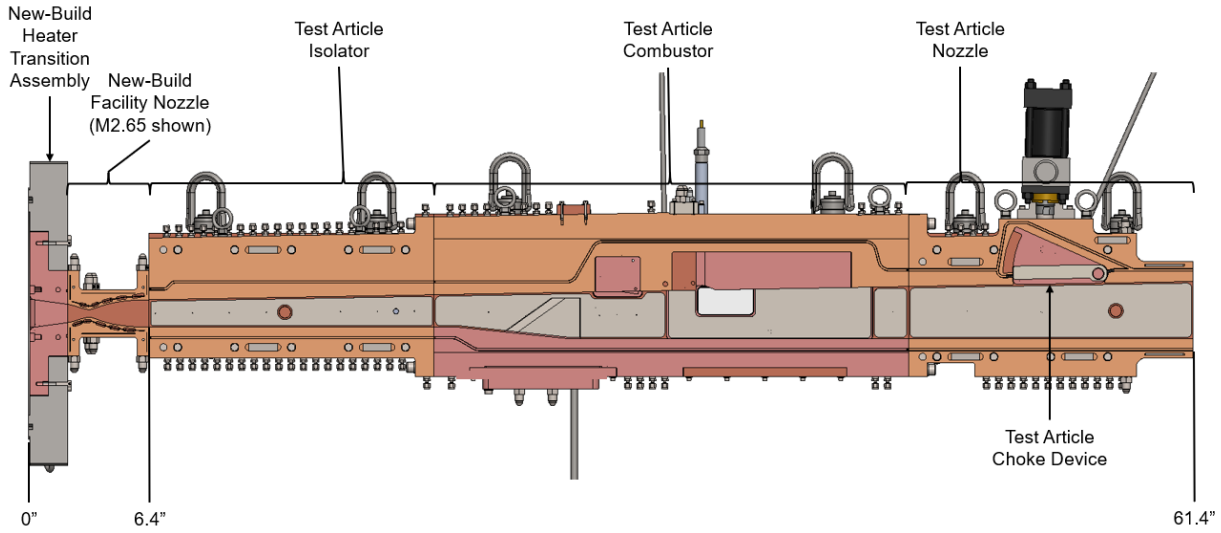


Figure 5: 0.5X scale test article with facility nozzle

MATERIALS SELECTION

The vast majority of components on both test articles are made from copper alloys, either wrought C10100 OFHC copper, wrought C18150 copper chromium zirconium, or printed GRCop-42 copper chromium niobium. Copper's high thermal conductivity allows heat to distribute throughout the part and reduce thermal gradients, thus reducing thermal strain. Most of the fixed flowpath components, as well as the Step FIBs, are made from C10100, while the Cavity Blocks, access panels, and combustor body-side wall are made from C18150 due to the higher strength required for these parts at elevated temperatures. GRCop-42 is used for the Strut and Ramp FIBs as well as the choke device due to the complex internal routing required for fuel and cooling. Some components away from the flowpath are made from aluminum or, for applications such as the support brackets that require greater strength, stainless steel. All test article windows will be machined from fused silica with their accompanying blanks made of C10100 copper.

One disadvantage of copper's conductivity is the loss of heat from the flow into the parts that make up the flowpath. To counter this and improve the survivability of the parts, the flowpath surfaces are plasma sprayed with a Yittria-Stabilized Zirconia (7YSZ) thermal barrier coating. For most components, this coating is applied in pockets machined into the flowpath surface, to control coating thickness and to protect the edges. On the struts, which are too thin for such pockets, the overall dimensions of the copper have been reduced by the thickness of the coating so that the coated part matched the nominal flowpath inner mold line.

MODULAR COMPONENTS

Each test article has four sets of modular components. From upstream to downstream, these are the Strut FIB, Ramp FIB, Step FIB, and Cavity Block. Each block comes in gaseous fuel, low-q liquid fuel, and high-q liquid fuel variants. The two upstream blocks also have a blank gaseous block as a spare without injectors, in case their diameters need to be changed from the baseline. There are also sets of defeatured variants of the upstream blocks to reduce flowpath blockage if deemed necessary. The low-q and high-q liquid FIBs differ in their injector diameters, with the high-q injectors having twice the area of their low-q counterparts, the smallest examples having diameters of 0.0055 in and 0.0028 in respectively. A breakdown of quantities provided for each FIB may be found in Table 1.

FIB	Gaseous	Gaseous Blank	Liquid, Low-q	Liquid, High-q	Blank	Defeatured
Strut	2x3	1x3	1x3	1x3	1x3	1x3
Ramp	2	1	1	1	0	1
Step	3x3	0	1x3	1x3	0	0
Cavity	1x9	0	0	0	0	0

Table 1: Number of fuel injector block variants to be acquired for each modular component per test article

Each gaseous fuel injector block has a single array of injectors, while each liquid block has two arrays, one with larger injectors, fed by independently controlled plenums. The liquid injectors were split into two arrays to allow for better control over a large range of mass flows while maintaining enough pressure to achieve sufficiently small fuel droplet sizes to promote evaporation in the combustor and avoid combustor blowout at lower fuel mass flow rates. A liquid fuel test will start with both injectors providing their maximum mass flow. Both the small and large injectors' flowrates will be varied within the fuel system capabilities that are limited by the maximum fuel supply pressure and the minimum fuel pressure that will provide the desired fuel particle sizes. Using these pressure requirements, the small and large fuel injector flowrate will be programed prior to the test to provide a smoothly decreasing fuel flowrate to the combustor until lean blowout occurs.

Strut Fuel Injector Blocks

The Strut FIB is the primary source of fuel for the test article, providing over half of the total fuel injection. Its design consists of a printed GRCop-42 holder block with three slots for strut blocks of the same material. Additional options for the strut block are blanks and defeatured “strutless” blocks which are also printed from the same material. The strutless blocks eschew the strut and replace the former’s array of injectors with a single large fuel port. The blank blocks contain neither struts nor fuel injectors and sit flush with the flowpath. The blank and strutless blocks are provided as a contingency measure in the event the struts create too much blockage, allowing runs with two, one, or no struts instead of all three. Figure 6 depicts the 2X scale Strut FIB with three gaseous or three strutless blocks installed in the holder.

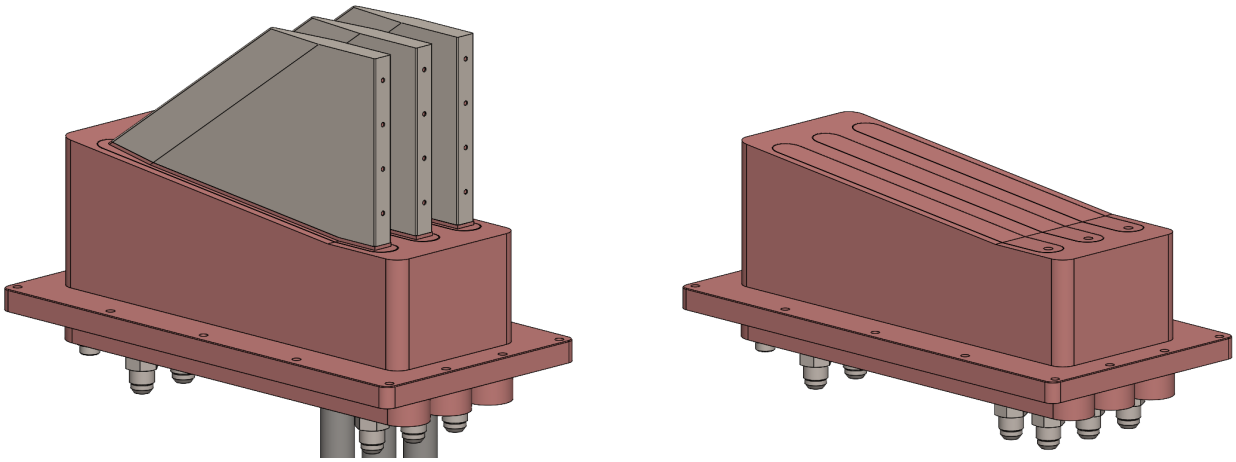


Figure 6: Representative examples of the Strut fuel injector block with gaseous struts (left) and “strutless” inserts (right) installed. Both examples shown here are for the 2X scale test article

The strut, blank, and strutless blocks were designed as individual components to allow the application of a thermal barrier coating to the struts without obstructions as would be the case if the struts were integral parts of the block. GRCop-42 was selected as the material due to its greater strength at high temperature, which was deemed critical for the relatively thin struts. Installation and removal are performed through the cowl-side surface.

Ramp Fuel Injector Blocks

Like the Strut FIB, the Ramp FIB is of printed GRCop-42 construction. Unlike the Strut FIB, the Ramp FIB is a single monobloc part with integral fuel injection with four variants. In addition to the standard three configurations noted above, a defeatured “rampless” block is provided. Like its strutless counterpart, the rampless block was designed to reduce blockage if this is observed to be a problem and features three large injector ports for gaseous fuel. The two liquid-fuel blocks feed their injectors from plenums, while the gaseous and rampless blocks have individual feeds for each injector to ensure equal flow across the full span of the flowpath. The Ramp FIBs are inserted and removed through the starboard sidewall of each test article. A liquid-fuel Ramp FIB and the gaseous rampless FIB may be seen in Figure 7.

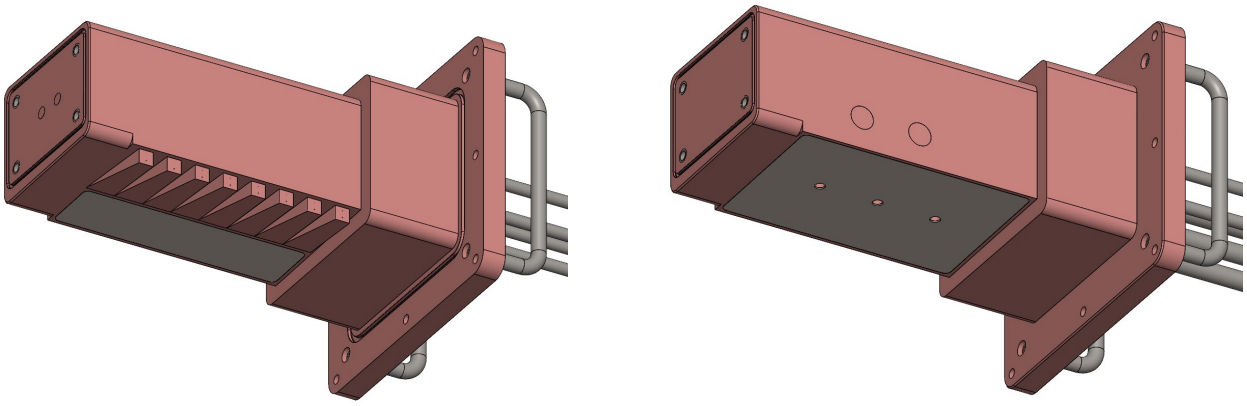


Figure 7: Representative examples of the Ramp fuel injector block for the 2X scale test article. The left shows the high-q liquid fuel block while the right shows the “rampless” block.

Step Fuel Injector Blocks

Each test article is provided with nine variants of the Step FIB, each conventionally machined from C10100 copper. This is broken down into three cavity heights and three different fuel types for each height. For the gaseous fuels, the injectors are drilled into the downstream face of the step, immediately under the ledge of the step. Due to the small diameters of the liquid fuel injectors, and the required distance between the plenums and the downstream face, a set of brazed blocks are installed into the downstream face. These feature a large diameter feed tube for each individual liquid injector with a jog allowing all injectors to be placed as close to the step ledge as possible. Each step block includes further injections ports for hydrogen as part of the ignition system, located just above the cavity floor. Figure 8 shows gaseous and liquid variants of the step blocks for the tallest cavities.

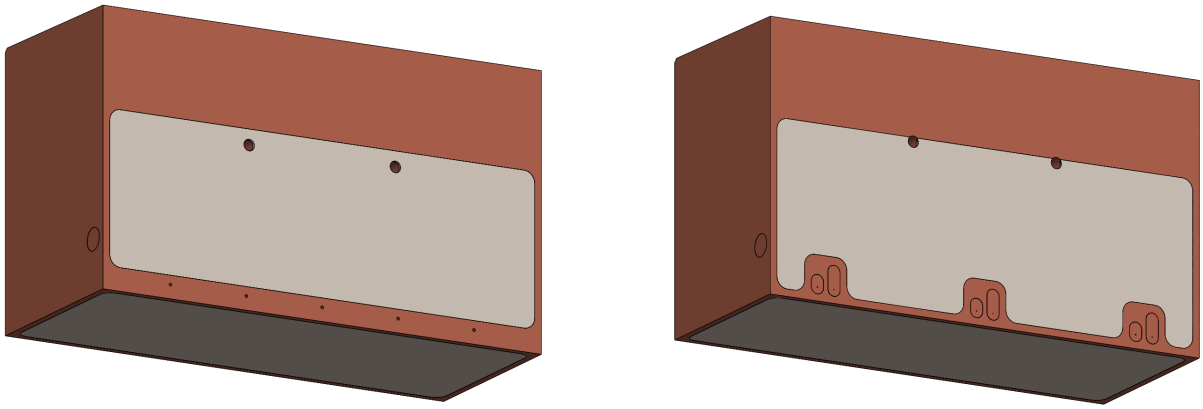


Figure 8: The gaseous fuel (left) and high-q liquid fuel (right) Step fuel injector blocks used with the largest cavities on the 2X scale test article. The pair of large ports are for H2 for the ignition system.

In order to improve accessibility to the various feed and return lines on the step block, a pair of spacer blocks is provided for each test article, one for each for gaseous and liquid fuels. This is inserted through the body-side wall to meet the Step FIB, which is installed via the access panels on either side of the combustor.

Cavity Blocks

The Cavity Blocks are the core of TC-3, creating all of the various cavity geometries being investigated. Each test article is provided with nine Cavity Blocks with varying combinations of height and length. The largest of these for the 2X scale test article is depicted in Figure 9. Each Cavity Block consists of two parts, one upstream for the cavity floor and one downstream for the cavity closeout. The latter is produced separately to simplify machining of an array of fuel injectors sited just above the cavity floor. Unlike the other fuel injector blocks, the Cavity Blocks are designed to be used only for gaseous fuel injection and will be unfueled for liquid fuel testing. Both sections of the Cavity Block are conventionally machined from C18150 copper and installation is performed through the combustor access panels.

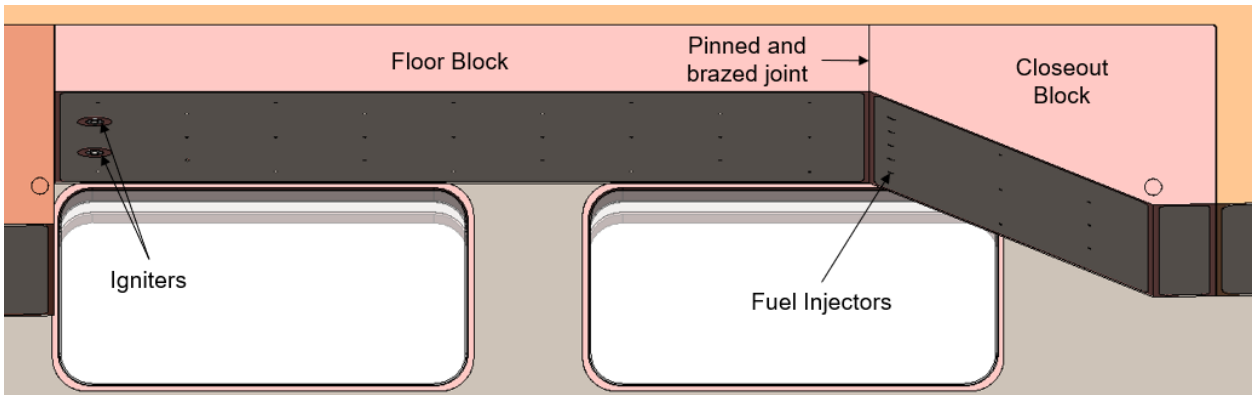


Figure 9: The largest cavity on the 2X scale test article. Note the row of injector ports near the base of the cavity closeout ramp and the two igniter stations at the upstream end near the step.

Each cavity block has one (0.5X Scale) or two (2X Scale) through hole(s) for a COTS ignitor to protrude into the flowpath. This ignitor features a single long electrode which will arc to the surrounding copper to light the hydrogen from the Step FIB. This concept was designed to allow easier access and routing for the igniter as a more conventional spark igniter, threaded directly into the cavity block, would be positioned in a narrow cutout up to five inches deep depending on the cavity. Each test article has a set of three spacer blocks for the igniter to accommodate each cavity height, as well as three ceramic sleeves to prevent the electrode from arcing away from the flowpath. The 0.5X scale version of this arrangement can be seen in Figure 10.

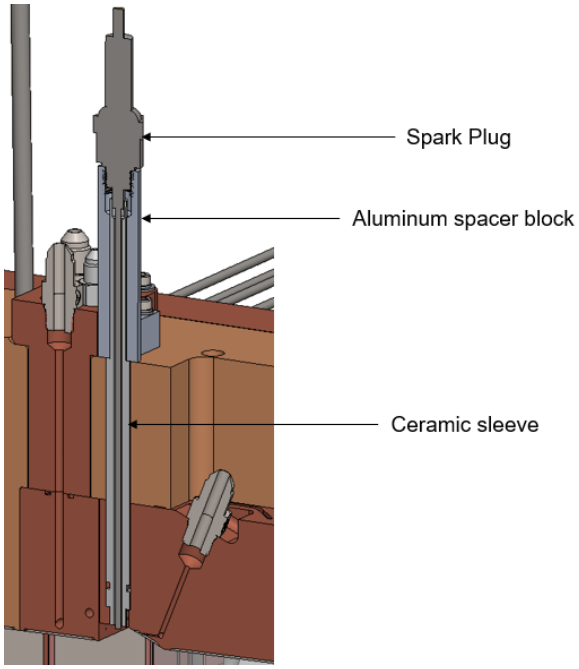


Figure 10: Section view through the igniter installation on the smaller test article for the smallest cavity geometry. Each cavity height requires its own spacer block and ceramic sleeve.

ACTUATION

Each test article is fitted with a wedge-shaped, printed GRCop-42 choke device on its body-side flowpath to provide backpressure prior to ignition. Its design was informed by work done for a previous test article design for LaRC by North Wind, where the concept was validated by CFD analysis performed by NASA. The choke device is actuated with a hydraulic cylinder with an operating pressure of 3000 psi on the 2X Scale test article and 1000 psi on the 0.5X Scale. The stroke of the cylinders is sized such that the choke device cannot be overextended to overpressure or unstart the test article. Should the linkage fail, a hardstop is incorporated onto the leading edge to catch the choke device before it can fall into the flowpath and cause damage; this can be seen in Figure 11. The shafts are held by a graphite-lubricated bronze bushing in each sidewall. The angular position of the choke device will be measured with a rotary encoder whose rotor is mounted to the end of the starboard shaft and whose stator is mounted to the sidewall. The port-side shaft includes provisions for mounting an AMS module for calibration purposes.

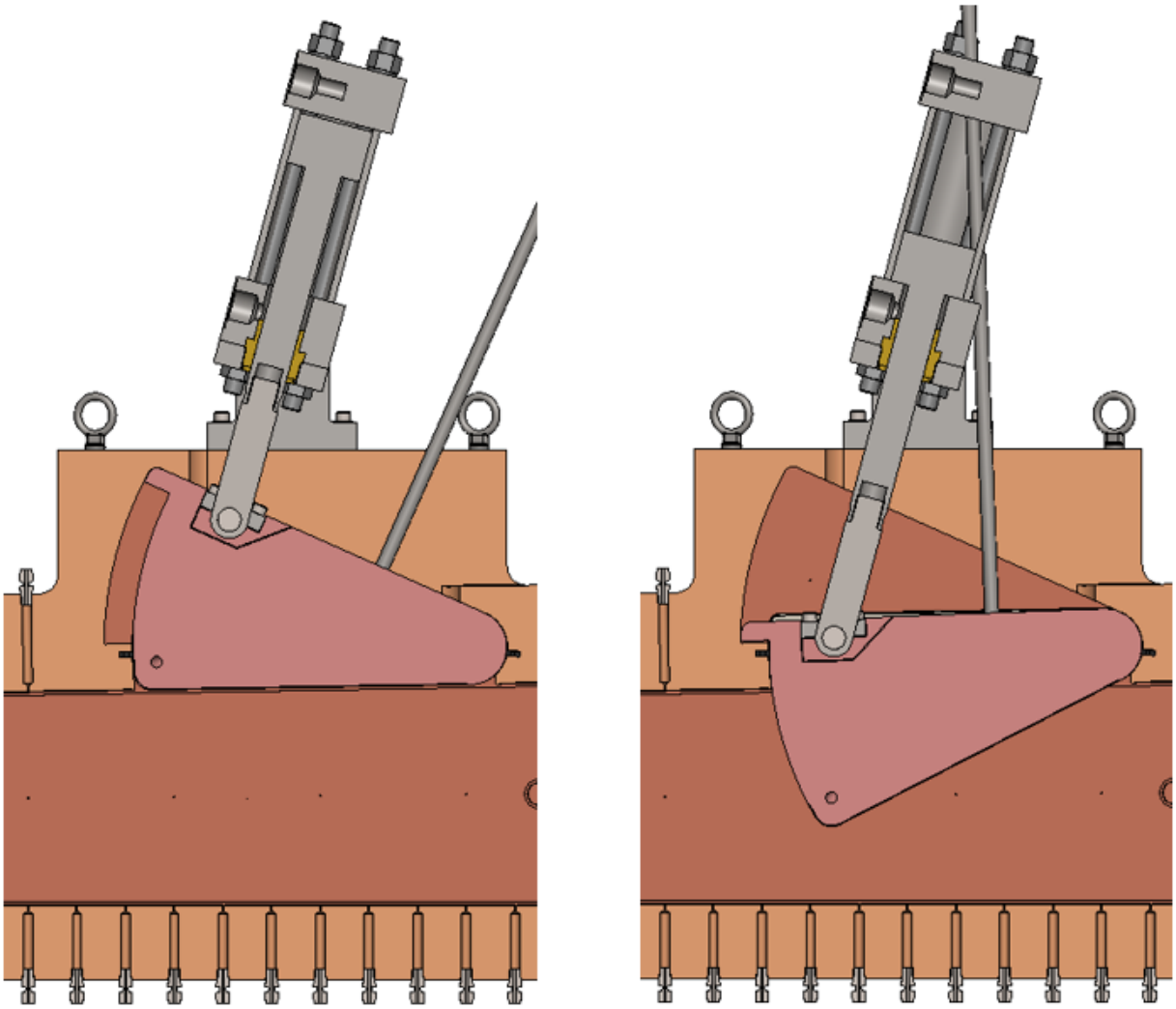


Figure 11: Section view through the 2X scale choke device showing its undeployed position on the left and its maximum deployment on the right.

SEALING

Most of the sealing on each test article is provided by Viton high-temperature elastomeric O-rings or cord stock. The length of each subassembly is sealed with a single piece of cordstock at each sidewall interface, with a second elastomer groove running around the flowpath at each subassembly interface. Care was taken to ensure that each axial cordstock groove meets the “radial” cordstock correctly to prevent leaks. Some of the modular components use a gland style arrangement with the elastomer wrapped around the base of a flange and compressed in a chamfer around the perimeter of the corresponding cutout. The windows and blanks are each provided with a pair of mica gaskets, one at the interface with the outboard portion of its frame and one at the interface with the inboard portion. These provide sealing while also cushioning the window to mitigate thermal strain and cracking during testing. A mica gasket also provides sealing under the cavity blocks as this region is too hot for elastomer seals.

For the actuated choke devices, a more complex solution was required. The design of the seals was developed with input from the NASA Glenn Research Center (GRC) seals group. The leading edge and the spanwise hinge are sealed with a set of graphite packings, with further layers of packing wrapped around the shafts between the flowpath and the bushings. To seal the sides of the choke device, a spring-loaded Inconel 625 bar with a nickel plating for added lubricity is submerged in a pocket in each sidewall and kept preloaded against the choke device by three die springs each. A section view showing the choke device sealing arrangement may be seen in Figure 12.

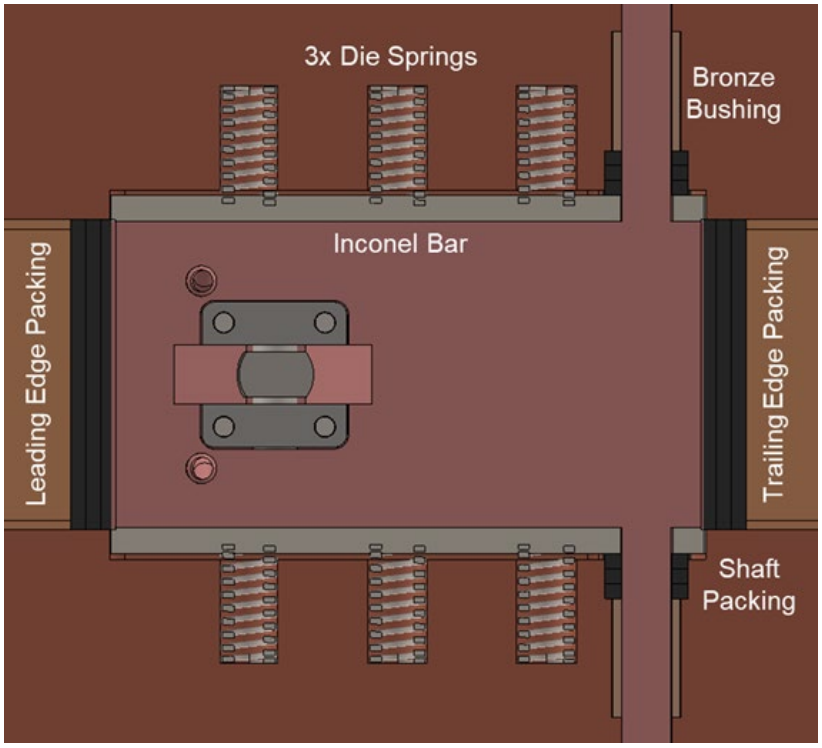


Figure 12: Section view of choke device sealing arrangements; 0.5X Scale example shown

INSTRUMENTATION AND OPTICS

Each test article is fitted with an array of instrumentation to monitor the flowpath. The majority of these are pressure taps that are fitted on each fixed flowpath component and on each cavity block. Each pressure tap consists of a stainless steel tube routed from the test article to the facility's pressure sensing modules. On the fixed components, these are connected via Swagelok fittings threaded into the outboard surface, while on the Cavity Blocks, the tubing is brazed to the block and routed along the back towards the centerline before being directed through a cutout in the body-side wall. The pressure taps on the floor of the cavity may be repurposed to enable fuel-air ratio measurements using the same methodology as Ombrello and Hammack [2] with each cavity having at least two pressure tap ports for this purpose. Each test article additionally has eighteen Medtherm TCS-E coaxial thermocouples on the fixed sections of the flowpath, positioned to be in contact with the back of the TBC coating. One further pressure tap and thermocouple is fitted to each sidewall behind the choke device seals as a health monitoring measure. A small number of Kulite high frequency pressure transducers on the fixed components and Medtherm heat flux gauges on the Cavity Blocks rounds out the flowpath instrumentation. Table 1 shows the complete lists of flowpath instrumentation for the test articles as a whole while the cavity blocks alone can be found in Tables 2 and 3 respectively.

Instrument Type	2X Scale	0.5X Scale
Pressure Tap	232-236	185-191
Coaxial Thermocouple	18	18
High-Frequency Pressure Sensor	3	2
Heat Flux Transducer	1-2	0-1

Table 2: Instrumentation counts for the two test articles. Note the range of pressure taps and heat flux transducers noted as these vary with the specific cavity installed on the test article

2X Scale					
Cavity		Overall		Cavity Floor	
H	L/H	PTs	HFTs	PTs	HFTs
0.5	3	31	1	2	0
0.5	5	28	1	2	0
0.5	7	29	2	4	1
1	3	28	1	2	0
1	5	27	2	7	1
1	7	27	2	10	1
2	3	27	2	7	1
2	5	29	1	16	1
2	7	31	1	25	1

0.5X Scale					
Cavity		Overall		Cavity Floor	
H	L/H	PTs	HFTs	PTs	HFTs
0.25	3	23	1	2	0
0.25	5	26	1	2	0
0.25	7	25	1	4	0
0.5	3	23	1	2	0
0.5	5	25	1	7	0
0.5	7	24	1	10	0
1	3	25	1	7	0
1	5	25	0	16	0
1	7	27	0	25	0

Table 3: Instrumentation counts for each cavity on the 2X Scale (left) and 0.5X Scale (right) test articles

Optical access to the test articles consists of a set of windows around the cavity and an additional window upstream at the trailing edge of the struts. The former consists of one or two windows on the cowl-side wall and each access panel to allow schlieren experiments and infra-red spectroscopy and imaging. The number and positions of the access panel windows vary with cavity height to minimize the degree to which the cavity block overlaps the windows and thus mitigate the thermal gradient experienced by the glass. This requires each test article to have three pairs of access panels as can be seen in Figure 13. In addition to the windows shown in Figure 13, a window was also place upstream of the cavity on the body-side wall at the strut trailing edge to be used to check for flameholding on the trailing edges of the struts. Each window is provided with a C10100 copper blank for experiments in which windows are not required.

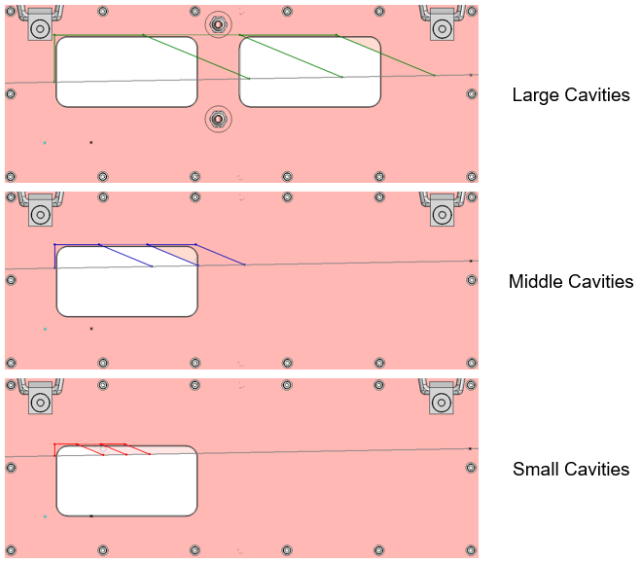


Figure 13: The three access panel configurations required to observe all nine cavities, with outlines of the relevant cavities overlaid

Outside of the flowpath, the fluid systems receive further instrumentation. Each fuel feed line has a single cross-shaped fitting immediately upstream of the entrance to the part with a pressure tap and thermocouple. The water-cooling system has a similar arrangement on the return line of each circuit immediately downstream of the part.

THERMAL SURVIVABILITY AND HEALTH MONITORING

As noted above, almost the entirety of the flowpath surface is covered by a 7YSZ thermal barrier coating (TBC). This coating serves the dual purpose of improving the survivability of the copper parts while keeping as much heat as possible in the flow to improve performance. The health of this coating is primarily monitored by visual inspection between tests with borescope ports in the Isolator and Nozzle subassemblies as well as the windows in the combustor section. During a test run, the health of the TBC can be monitored via readings from the flowpath thermocouples, and the exit temperature can be measured on the cooling water return lines. In the event of TBC ablation, all modular components, the choke device, and the fixed flowpath walls can be uninstalled from the test article to be recoated.

A number of components, including the majority of the modular ones, feature active water cooling to deal with local hotspots identified during thermal analysis. These are fed from two sources, the standard DCSCTF 500 psi water system and a higher-pressure 1500 psi system that is to be installed in the DCSCTF as part of another project that will run in the near future prior to TC-3. The pressure transducers and heat flux gauges have their own additional cooling circuits fed by low pressure (45-55 psi) water manifold. Tables 4 and 5 show a breakdown of the test article cooling circuits using the facility standard and high-pressure water manifolds.

Facility Test Article Manifold			
	Circuit	Flow Rate (lbm/s)	Flow Rate (GPM)
2X Scale Test Article	Heater Transition Flange - US	2	14.4
	Heater Transition Flange - DS	2	14.4
	Body-Side Combustor	0.7	5.04
	Cavity Step FIB	0.35	2.52
	Nozzle Body-Side	0.5	3.6
	Nozzle Cowl Side	0.5	3.6
	Nozzle Port Side	0.5	3.6
	Nozzle Starboard Side	0.5	3.6
	SUM	7.05	50.76

Facility Test Article Manifold			
	Circuit	Flow Rate (lbm/s)	Flow Rate (GPM)
0.5X Scale Test Article	Heater Transition Flange - US	0.75	5.4
	Heater Transition Flange - DS	0.75	5.4
	Body-Side Combustor	0.7	5.04
	Cavity Step FIB	0.25	1.8
	Nozzle Body-Side	0.25	1.8
	Nozzle Cowl Side	0.25	1.8
	Nozzle Port Side	0.25	1.8
	Nozzle Starboard Side	0.25	1.8
	SUM	3.45	24.84

Tables 4: Cooling circuits on the large (left) and small (right) test articles using the facility manifold

High Pressure Manifold			
	Circuit	Flow Rate (lbm/s)	Flow Rate (GPM)
2X Scale Test Article	Strut FIB Circuit 1	0.7	5.04
	Strut FIB Circuit 2	0.7	5.04
	Strut FIB Circuit 3	0.7	5.04
	Ramp FIB	0.5	3.6
	Cavity Block	0.2	1.44
	Port Access Panel	0.6	4.32
	Starboard Access Panel	0.6	4.32
	Choke Device	1.35	9.72
	SUM	5.35	38.52

High Pressure Manifold			
	Circuit	Flow Rate (lbm/s)	Flow Rate (GPM)
0.5X Scale Test Article	Strut FIB Circuit 1	0.2	1.44
	Strut FIB Circuit 2	0.2	1.44
	Strut FIB Circuit 3	0.2	1.44
	Ramp FIB	0.3	2.16
	Cavity Block	0.075	0.54
	Port Access Panel	0.3	2.16
	Starboard Access Panel	0.3	2.16
	Choke Device	0.75	5.4
	SUM	2.325	16.74

Table 5: Cooling circuits on the large (left) and small (right) test articles using the high-pressure manifold

TEST ARTICLE THERMAL AND STRUCTURAL ANALYSIS

The above mechanical design was supported by thermal and structural analysis using flowpath aerothermal CFD loads provided by NASA. Although loads were provided for several conditions and configurations, most of the analysis was focused on two cases to accommodate project schedule. These were a combined thermal-structural analysis for the M7 high-q condition with H2 fuel and a pressure-only structural analysis for the M6 high-q condition with maximum backpressure. Both studies were conducted on the larger test article with the largest cavity. Additional analysis was performed to validate the design of the new-build nozzles, and the ejector transition ducts, but this paper will focus its discussion on the test article analysis.

Hydrogen was down-selected as the fuel of interest early on as it was expected to produce the hottest combustion and the highest heat loads; this was validated by a comparison between the CFD loads provided for the other gaseous fuels of interest for a given test case and the resulting heat transfer coefficients (no CFD loads were provided or analyzed for the liquid fuels). The largest cavity was selected at the same time, as this was likewise expected to produce the highest heat loads while also providing the least mass to act as a heat sink, and was validated by comparison with another, smaller cavity configuration. The thermal-structural analysis effort was focused on the M7 test case after initial studies for both M7 and M6 showed the former was more thermally challenging despite the latter test running 15 seconds longer. After initial analysis was conducted on both the larger and smaller test article, attention was focused on the former after the smaller test article demonstrated more resilience to the loads provided, likely due to it having less exposed surface area while having relatively thicker walls on all components. Both test articles use 0.030 in thick TBC, giving the 0.5x scale more relative TBC volume. The Mach 6 pressure-only backpressure condition was studied as a worst-case structural scenario with maximum choke device deflection; this is not considered a likely operational condition by NASA.

GOVERNMENT FURNISHED CFD LOADS

All CFD loads provided by NASA were produced using the VULCAN CFD code [8] for a half-span test article geometry, and quarter symmetry solutions for the facility nozzles. These were interpolated by North Wind via Tecplot for use in ANSYS finite element analysis software. Transient thermal analysis consisted of a 15 second facility combustion air heater air-only ramp-up period followed by 45 seconds (M5 and M6) or 30 seconds (M7) combustion test. The combustion test's flame temperature was taken as constant, not accounting for local transient variations in temperature, the intended ramp-down of fueling during a test, or injectors being unused during a test. A notional test run at Mach 7 is shown in Figure 14. For the M6 pressure-only structural analysis, the maximum possible pressure calculated by NASA, 152psi, was applied to all flowpath surfaces including all other surfaces inboard of the seals.

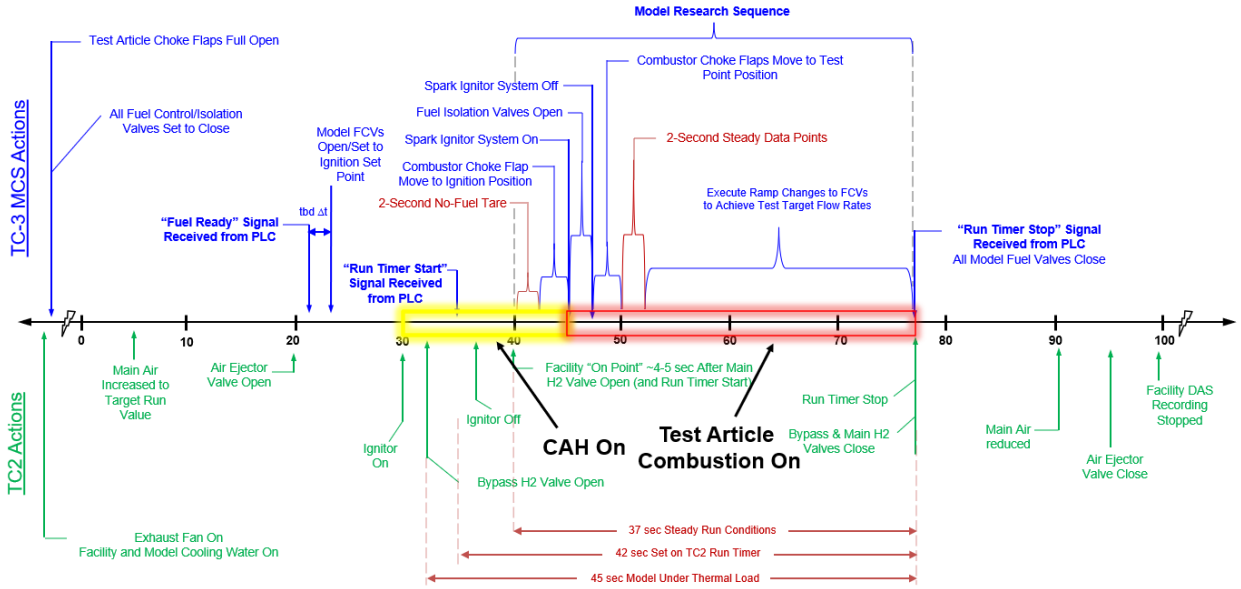


Figure 14: Notional timeline for a Mach 7 test run, with the air-on period highlighted and divided into heater-only and test article combustion segments. The lower-Mach tests are the same except for a longer (45 vs. 30 second) combustion period

The NASA-produced VULCAN CFD loads are interpolated in Tecplot using a 700 K cold wall assumption. Heat rate, Qdot [W], is GFI provided and is integrated along the flowpath surface area to find the heat flux at each station. Using Newton's Law of Cooling [3] to find heat transfer coefficient, the heat flux is divided by the difference in surface adiabatic wall temperature, Taw, and the isothermal wall temperature, Tiso, 700 K.

Figure 15 shows a plot of the adiabatic wall temperature surface loads with a peak temperature of 3148 K located on the downstream face of the strut fuel injector block. For the transient thermal analysis, the adiabatic wall temperatures are used in addition to the heat transfer coefficient (HTC) (Figure 16) in the convection boundary condition, which are mapped on all flowpath surfaces. A constant combustion air heater convection boundary condition is used for the first 15 seconds of run time. From the facility nozzle outflow conditions, a temperature of 2133 K and an HTC of 1295 W/m^2*K are used. Surface pressure loads are provided in Figure 17, though a conservative maximum pressure of 152 psia is applied in static structural analyses.

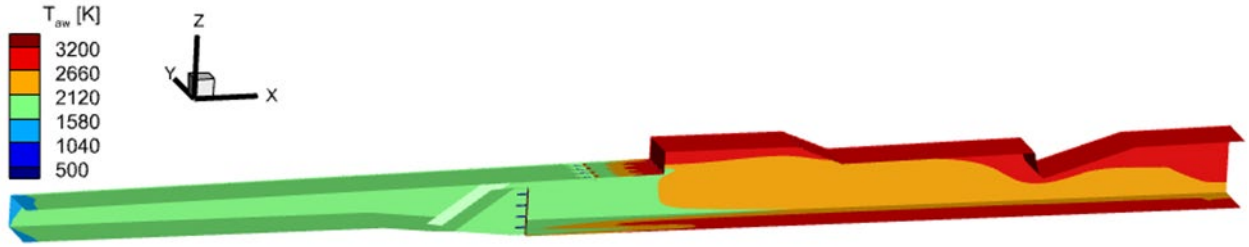


Figure 15: Adiabatic Wall Temperature plot of 2x scale, L14D2, Choke Flap 16.5 deg, Mach 7, q 1500 psf - H2 fuel phi=0.85 test article

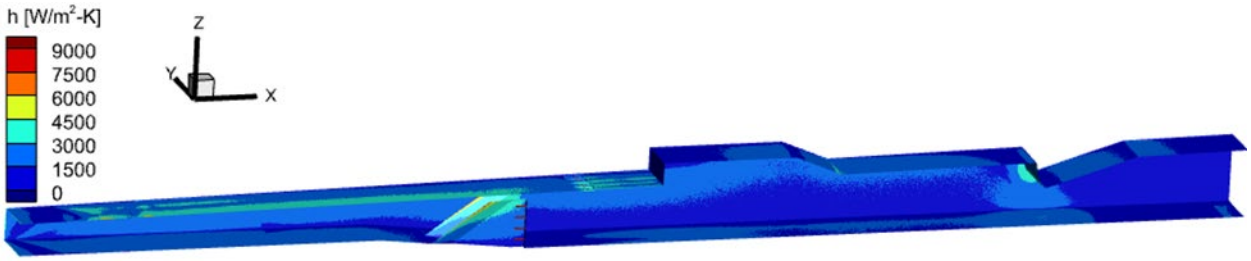


Figure 16: Heat Transfer Coefficient surface loads of 2x scale, L14D2, Choke Flap 16.5 deg, Mach 7, q 1500 psf - H2 fuel phi=0.85 test article

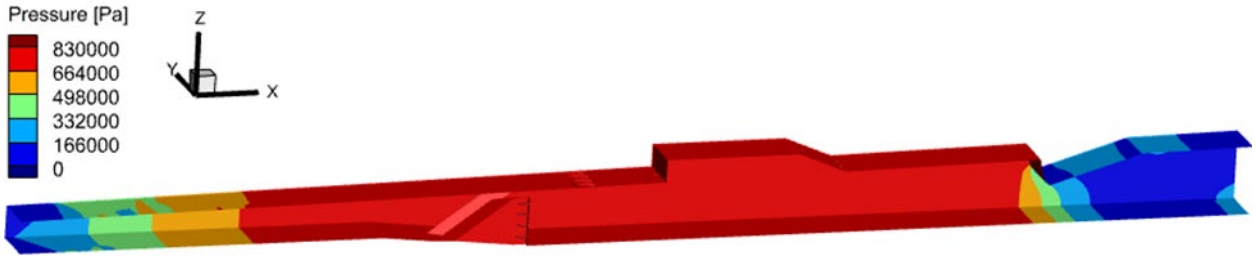


Figure 17: Surface pressure loads of 2x scale, L14D2, Choke Flap 16.5 deg, Mach 7, q 1500 psf - H2 fuel phi=0.85 test article

In addition to well defined test article surface loads, North Wind was provided with quarter symmetry 0.5x scale nozzle loads. Using the same methodology described above, adiabatic wall temperatures and HTCs were used in a convection boundary condition for each nozzle's transient thermal analysis. Surface pressure loads were applied to flowpath surfaces, including the heater transition flange, which was analyzed in addition to the nozzles. The test campaign includes 4 different nozzles, 0.5x scale M2.1, 0.5x scale M2.65, 2x scale M2.1, and 2x scale M2.65. NASA has already produced and tested the larger 2x scale nozzles; therefore, those analyses are not in the scope of this program. Each 0.5x scale nozzle is required to withstand the thermal structural loads and is included in the CDR level analysis. Both nozzles are tested at 2 different enthalpies, Mach 5 and 6 for the M2.1 nozzle, and Mach 6 and 7 for the M2.65 nozzle. Since the Mach 7 condition is the most extreme condition, those loads are shown below on the 0.5x scale M2.65 nozzle, Figures 18, 19, and 20.

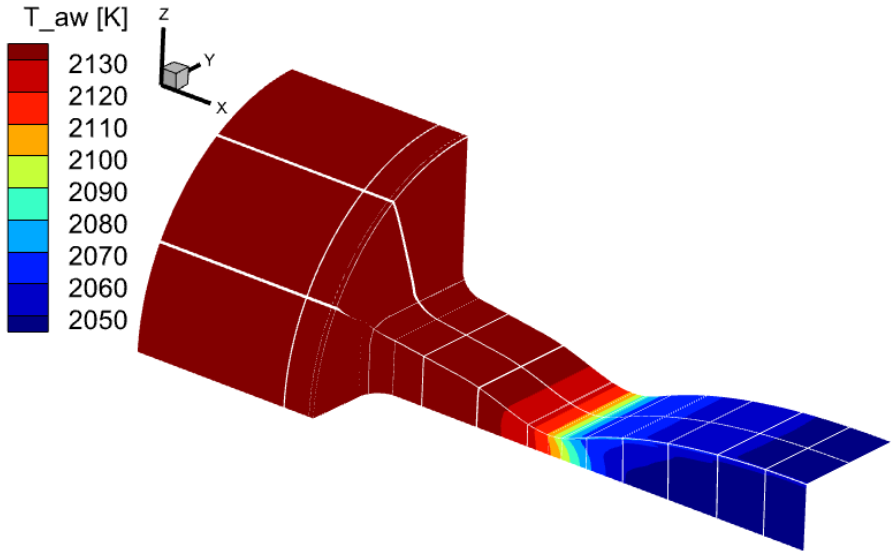


Figure 18: Adiabatic wall temperature plot of 0.5x scale M2.65 M7 q = 1500 psf nozzle

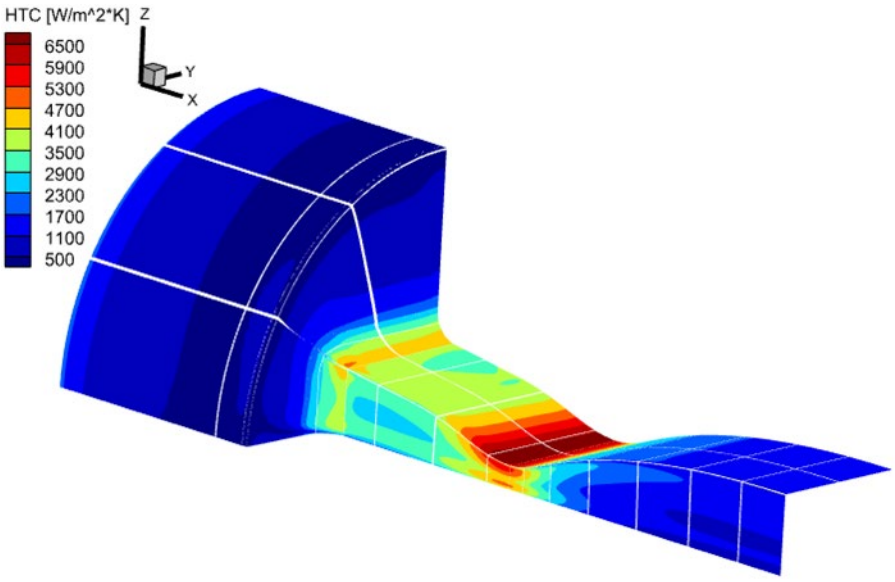


Figure 19: Heat transfer coefficient surface loads of 0.5x scale M2.65 M7 q = 1500 psf nozzle

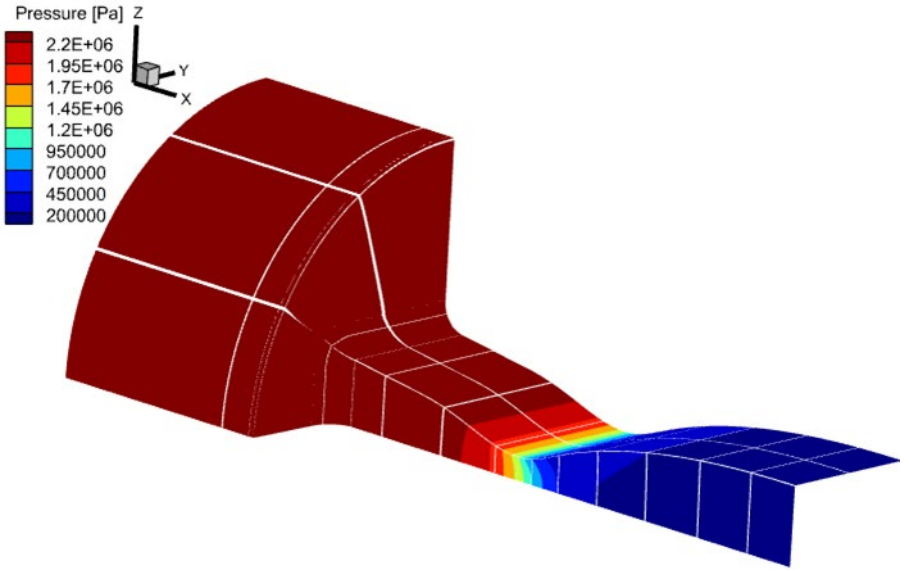


Figure 20: Surface pressure loads of 0.5x scale M2.65 M7 q = 1500 psf nozzle

TEST ARTICLE THERMAL ANALYSIS

Transient thermal analysis was completed in 2023 R2 Ansys Mechanical. Due to the nature of a direct-connect tunnel test, test article weight was limited only by the facility overhead rail load rating of 3,000 pounds. To stay within weight limits, heat sink copper materials were selected in addition to using active water cooling. For parts facing the most extreme thermal and structural conditions, GRCop-42 was used due to its high thermal conductivity, high strength, and ability to utilize additive manufacturing to print complicated cooling circuits [4]. For components where conventional machining was possible, C18150 copper chromium zirconium was selected. C18150 has the high thermal conductivity of a copper alloy, higher strength of a copper chromium, and improved performance at high operating temperatures from the addition of zirconium [5]. For the overall test article, C10100 Oxygen Free High Conductivity (OFHC) copper is used due to the material's optimal thermal conductivity.

The thermal analysis model uses bonded contacts with thermal interface conductance values determined from material contact pairs. The GFI provided CFD loads are imported from Tecplot onto each flowpath surface, shown in Figures 20 and 21. Active cooling passages are designed to keep peak temperatures within material limits, each highlighted in Figure 22. Additive manufacturing is used in components where conventional machining is not possible, such as the choke flap, ramp fuel injector block, and strut fuel injectors. Other cooling locations such as the downstream nozzle circuits, cavity and step blocks, access panels, and body-side wall, use conventional machining techniques to drill circular cross section cooling channels. Inflow cooling water temperature is kept at room temperature in DCSCTF. An iterative process is used to determine cooling mass flow rate, and therefore convective heat transfer coefficient of the coolant water. A modified version of the Dittus-Boelter equation [6] is used, from inputs including channel hydraulic diameter, mass flow rate, and pressure to calculate convective heat transfer coefficient as a function of temperature. This HTC is applied along the surface of every cooling channel in addition to an inlet temperature and corresponding mass flow rate for each cooling boundary condition.

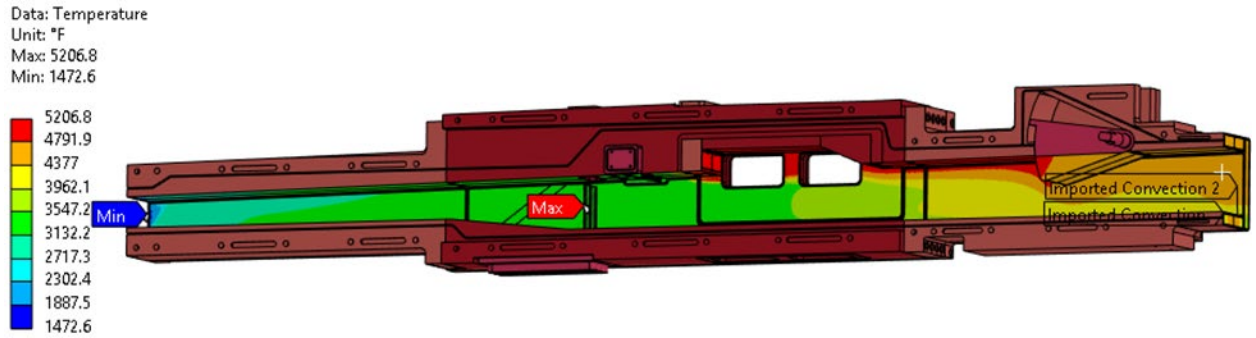


Figure 21: Adiabatic wall temperature surface loads applied as convection boundary condition on analysis model in Ansys

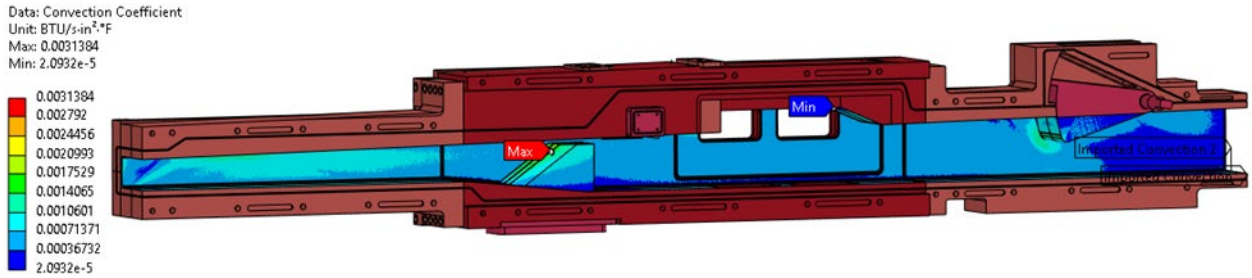


Figure 22: Heat Transfer Coefficient surface loads applied as convective boundary condition on analysis model in Ansys

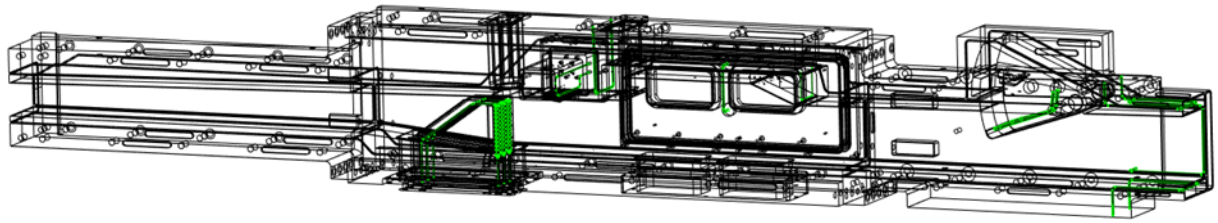


Figure 23: Cooling circuits highlighted in green

The results from the transient thermal analysis are used to determine component survivability at the most rigorous test condition. The pressure drop across each cooling circuit is calculated to ensure enough flow is being delivered to eliminate the chance of local boiling by keeping cooling circuit wall temperatures below local saturation temperatures. All 7YSZ temperatures must remain below the local maximum allowable temperature of 4,300 °F. Maximum TBC temperatures are shown in Figures 23, 24, and 25 below which illustrates the overall temperatures of the 2x scale M7 test article at the conclusion of a test run in different view angles. The maximum surface temperature is located on the step block downstream of a fuel injector hole. All TBC bodies remain within material limits with acceptable margin.

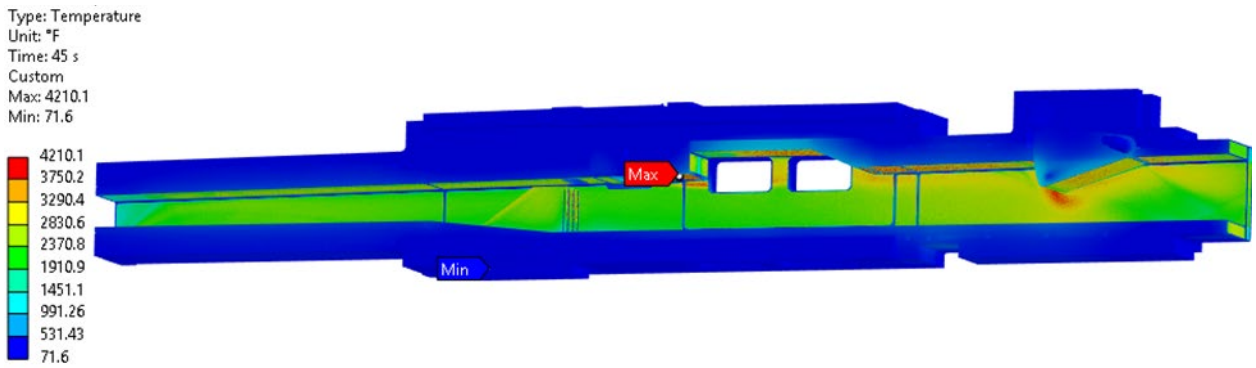


Figure 23: Overall temperature, sidewall removed for clarity

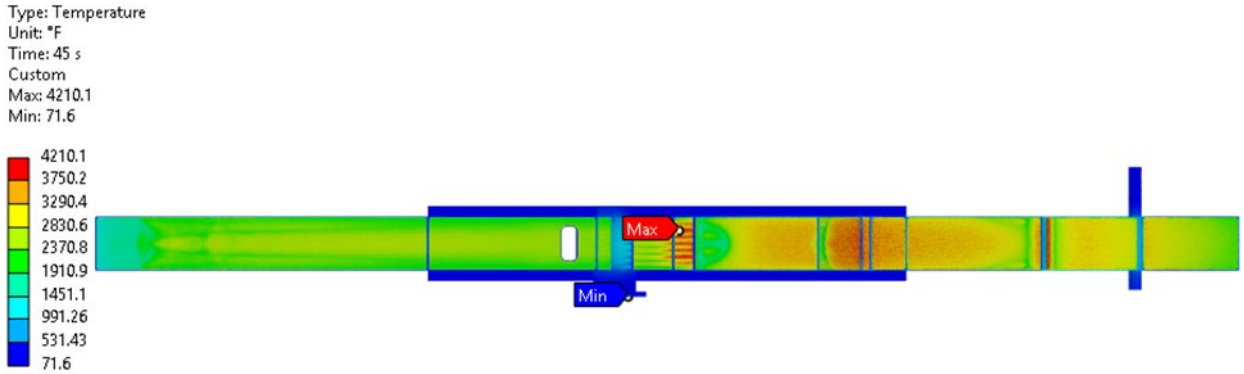


Figure 24: Overall temperature, body side walls

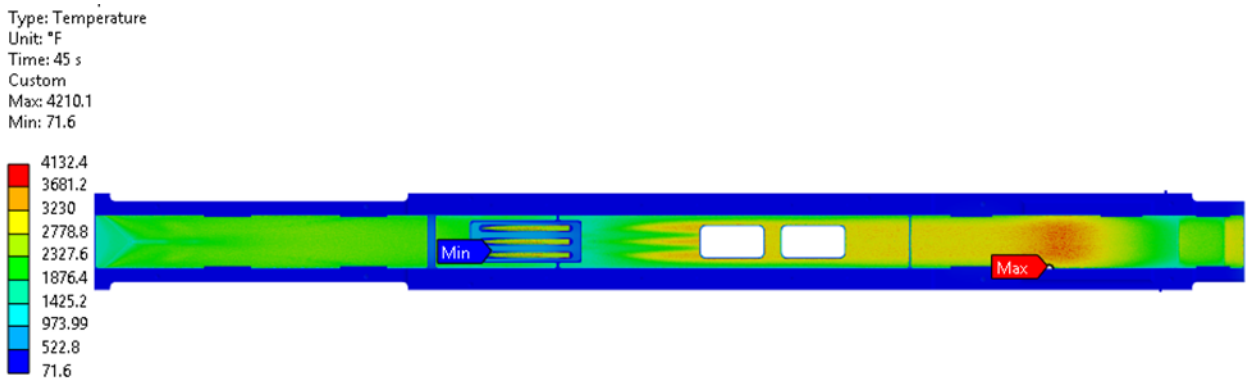


Figure 25: Overall temperature, cowl side walls

Copper temperatures are shown without TBC bodies included (Figure 26) to more accurately represent the color scale. The maximum copper temperature under the TBC is located at the peak of the choke flap. This component is GRCop-42 material and has a maximum service temperature of more than 1,400 °F [4], giving margin on material allowable temperature. Peak thermal response is expected in this region due to the actuated choke flap creating a mechanical throat, producing high heat transfer coefficients and temperatures. A second region of interest is the thin strut fuel injector blocks. The gaseous fuel configuration of these components utilize a double cooling channel design with elliptical cross sections. Each circuit surrounds the fuel injector holes to ensure thin-walled sections stay within material temperature limits, shown in Figures 27, and 28. By using this cooling scheme, the maximum metal temperature is 1,145 °F, with the peak located in the thickest region of the part. The removable cavity block is also a thin component in this configuration. The large combustor configuration is constructed from a 1 in thick removable cavity block machined from C18150. At Mach 7 enthalpy, the

resulting metal temperature on this thin block reaches a maximum of 1,120 °F. Copper chromium zirconium (C18150) has a maximum service temperature of upwards of 1,450 °F [5], giving this component acceptable margin on material temperature limits. All material and water temperatures are within allowable material limits at the end of the 45 second Mach 7 enthalpy test.

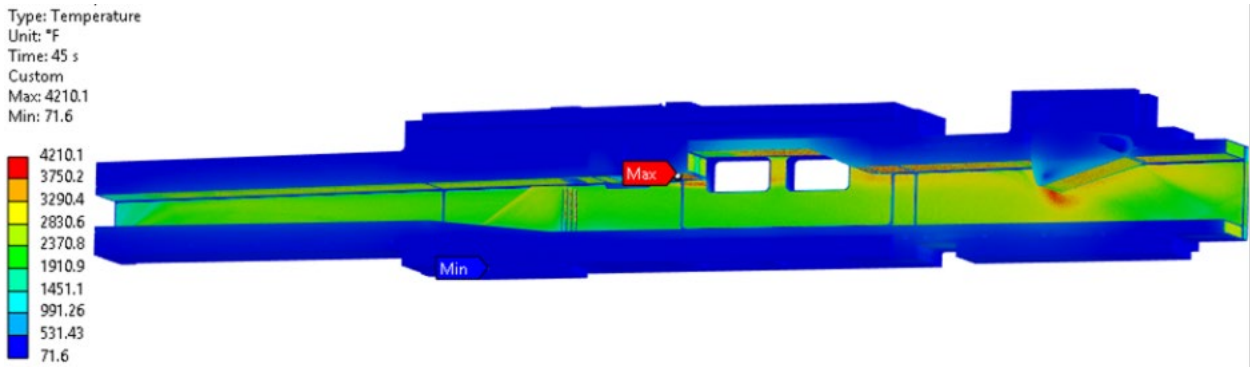


Figure 26: Copper only temperature, port sidewall removed for image clarity

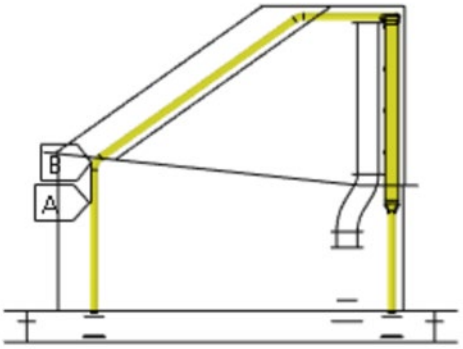


Figure 27: Side view of strut fuel injector block, highlighting cooling channel



Figure 28: Top-down view of strut FIB cooling channel, shown in Figure 27, cross sectional shape

THERMAL ANALYSIS CONCLUSION

A balance between copper heat sink materials, strategically placed TBC, and actively cooled components allow the modular test articles to survive the required enthalpies and test durations. In addition to the baseline gaseous fuel injector geometries, separate component level thermal analysis was conducted on liquid fuel injection geometries for each fueled component. All resulting metal and TBC temperatures were acceptable and within material limits. Hand calculations were done to compare the maximum heat loads, by comparing adiabatic wall temperatures and heat transfer coefficients, between gaseous hydrogen and ethylene-methane mixture fuel. As expected, the hydrogen fueling produced the most extreme surface loads with higher adiabatic wall temperatures and higher overall heat transfer coefficients. A smaller, mid-size cavity configuration, with a length of 5 in and depth of 1 in, was also run. This thermal analysis was run to validate the assumptions made prior that the largest 2x cavity configuration would yield the most rigorous thermal results. This assumption was in fact validated with subsequent thermal analysis. Lastly, the 0.5x scale large cavity test article was analyzed, once again confirming the 2x scale highest temperature assumption. Therefore, North Wind moved towards a Critical Design Review focusing on the most rigorous case: M7 q = 1500 psf 2x scale large cavity configuration

test article. Successful transient thermal analyses have been run to demonstrate the survivability of both 0.5x and 2x scale test articles at critical conditions.

TEST ARTICLE STRUCTURAL ANALYSIS

Two versions of static structural analyses were conducted for the worst case 2x scale large cavity M6 test article. The Mach 6 condition was determined to be the highest-pressure load after NASA internally calculated the resulting pressure due to maximum choke flap deployment for the highest possible test condition total pressure. Though this is not a test objective operating condition, this maximum pressure of 152 psia was used as a conservative boundary condition for all structural analysis.

The first version of structural analysis was to simulate pressure-only mechanical stresses in the test article. Applied loads in this analysis were the internal water-cooling pressures inside each channel, 1500 psi for high pressure circuits and 500psi for facility low pressure circuits, and 152 psi applied to all flowpath surfaces and all surfaces inboard of the seals. The selection of surfaces inboard of the seals were included to capture all possibilities of pressure distribution. The applied pressure load is ramped up across 3 different load steps to gradually increase force. Abruptly adding higher magnitude forces can produce errors in the mechanical solver. Remote forces are utilized to represent forces on window frames from pressure acting on glass windows, since the window bodies are not included in the finite element model. The test article is constrained by an upstream frictionless support (Figure 29) which anchors the upstream isolator section at X=0 in. The rest of the test article assembly is free to grow downstream. These upstream faces are also constrained in the Y and Z directions using remote displacements (Figure 30) which constrain each degree of translation, respectively. There are two stations along the test article water line where the overhead rail supports interface with the port and starboard sidewalls. These boundary conditions are also remote displacements with the vertical direction constrained, shown in Figure 31.

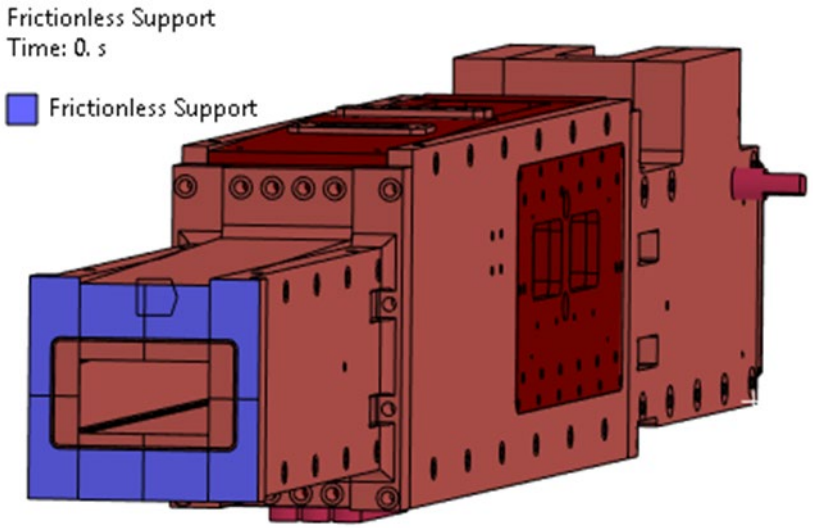


Figure 29: Upstream frictionless support, constrains downstream translation

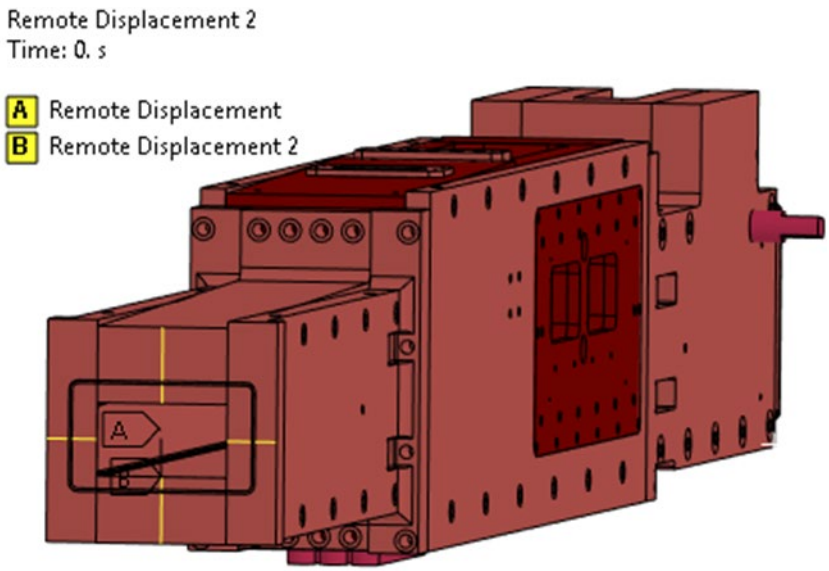


Figure 30: Remote displacement boundary condition constraining vertical and lateral displacement

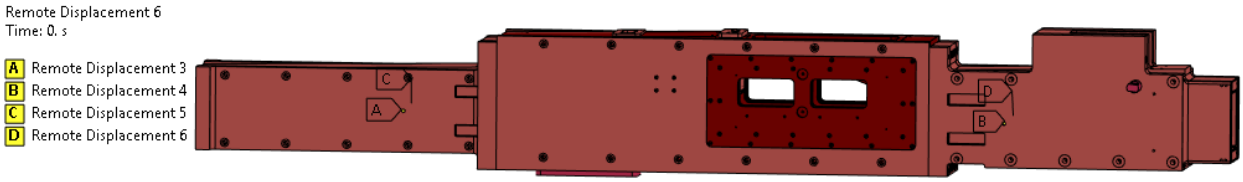


Figure 31: Remote displacement boundary conditions constraining vertical translation at support hanger interfaces

The structural model uses many different types of connections. Frictionless contacts are used between mechanically fastened components and subassemblies. Bonded contacts are used in parts that are brazed together. Beam elements are created to represent fasteners connecting components together across the test article. Cylindrical joints are used in pin locations. Cylindrical joints were chosen since the pins are free to rotate along the z (axial) axis and free to translate in the Z direction. No load is transferred axially along pins. Pin coordinate systems are shown in Figure 32 below. General joints are used at key locations and set to be free to translate in the X and Y direction and Z rotation. Each key is fixed vertically by fixing translation in the Z direction. Key coordinate systems are shown in Figure 33 below. Fixed joints are used between the choke flap port and starboard shafts and the sidewall female portion, located at the bushing locations. Joints are used to extract reaction forces at each joint location. Hand calculations utilize joint reaction forces to appropriately size pins, keys, and bushings throughout the test articles. Subassembly models are used for a more detailed structural analysis on the choke flap and strut fuel injector blocks. A combination of keys and pins are used for controlling flowpath position between subassemblies.

The pressure-only structural analysis results show equivalent maximum von-Mises stresses in each component. These resulting stresses are compared to material strengths at the corresponding local temperature to calculate safety factors on tensile yield strength and tensile ultimate strength. The pressure-only structural analysis is also used to determine static equilibrium across the test article. Standard handbook methods are used to confirm the model is balanced, fasteners have ample safety factors on tensile yield and ultimate strength, keys and pins have acceptable safety factors on shear strength, and that Helicoils have acceptable pullout strength safety factors for assembly.

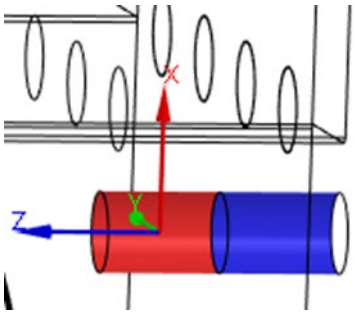


Figure 32: Pin joint coordinate system

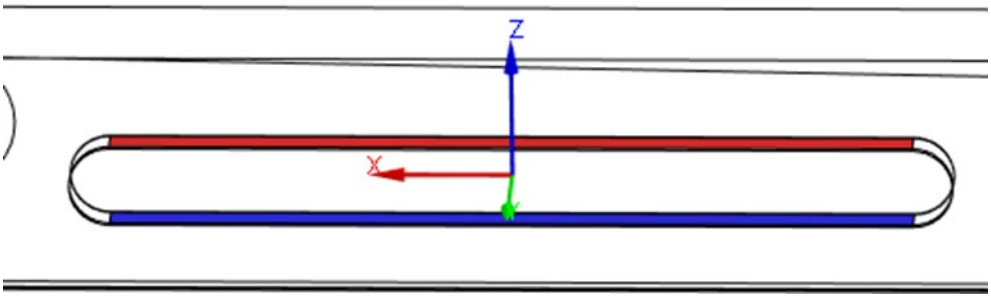


Figure 33: Key joint coordinate system

The second load case involves a combined thermal and pressure static structural analysis. The thermal results from transient thermal analysis were imported onto a structural model and applied on the same load step as the pressure boundary condition. There are two main goals of a combined thermal structural analysis like this: firstly, to calculate total deformation caused by combined thermal and pressure loads, and secondly, to calculate low cycle fatigue based on total strain results. The boundary conditions are identical to the pressure-only structural analysis except for the addition of the imported thermal loads. This analysis is run in multiple load steps. The first load step ramps up the thermal load application to avoid abruptly applying a large load and potentially encountering solver issues. The second load step holds the thermal loads steady and starts the pressure application ramp up, ramped for the same reason as previously described. The third, and final load step holds the thermal load constant and completes the pressure ramp up.

The final load step is the result containing full pressure and thermal loads. The end of the first load step represents thermal-only structural loads. Total strain and deformation were found using the combined thermal structural FEA solution from load step 3. Total strain is the sum of the equivalent thermal strain and equivalent elastic and plastic strains. For this project, plastic strain is negligible due to parts being designed to have stresses lower than each component's yield strength at temperature. The Coffin-Manson equation (Figure 34) [7] uses material inputs as a function of resultant part temperature, along with total strain, to compute low cycle fatigue to failure. Material inputs include percent reduction in area, Young's modulus, and tensile ultimate strength at temperature. Each component achieves an acceptable safety factor on cycles based on the requirement of 1,000 cycles per test article. It is important to note that the requirement for a duty cycle of 1,000 tests is across every test condition and test configuration. The fatigue cycles were all calculated assuming worst case Mach 7 enthalpy and Mach 6 pressure for all 1,000 cycles. Lower strains are expected at lower Mach conditions, resulting in overall increased life.

Total deformation results are provided back to the designer to incorporate appropriate cold gaps to allow for the expected thermal growth to occur without issues or interferences.

$$\varepsilon_t = 3.5\frac{S_t}{E}N^{-0.12} + \varepsilon_f^{0.6}N^{-0.6}$$

Figure 34: Coffin-Manson equation

STRUCTURAL ANALYSIS CONCLUSION

The structural analysis effort for the TC-3 test articles can be broken down into two separate analyses. Both analyses are integral to ensuring mechanical and thermal survivability of the worst-case Mach 7 thermal conditions and Mach 6 pressure. By combining thermal and structural loads, life cycles and total deformation can be calculated to alleviate thermal induced structural concerns. Pressure-only static structural analysis is useful in ensuring every component, fasteners, pins, keys, and Helicoils included, survive the rigorous pressure loads and meet safety factor requirements. This technique is also useful in ensuring the FEA model made by the analyst is in static equilibrium and there are no setup errors. By having insight from both methods of structural analysis, confidence is gained in test article survivability when tested against harsh Mach 7 conditions. Hand calculations, heritage designs, and finite element analysis are all coupled together to increase confidence in survival.

SUMMARY AND CONCLUSIONS

Mechanical design and supporting analysis for two modular test articles for NASA's Technical Challenge 3 have been completed to CDR readiness based on NASA-furnished CFD loads. The design of both test articles was informed by prior work on the direct connect test articles.

FUTURE WORK

Technical Challenge 3 will proceed to CDR in the January-February 2026 timeframe, with finalization of the drawing package to follow in the spring. Delivery of the first test article is expected to occur in the summer of 2028 with the second to follow twelve months later.

ACKNOWLEDGEMENTS

The authors would like to thank NASA for the opportunity to participate in Technical Challenge 3 under the RSES contract.

REFERENCES

[1] N. Hass, K. Cabell, A. Storch, and M. Gruber, "Summary of Ground Tests Supporting HIFiRE Flight 2: Hydrocarbon Fuels Testing and Direct-Connect Engine Tests", *JANNAF Journal of Propulsion and Energetics*, Vol. 6, No. 2, 2016

[2] T. Ombrello and S. Hammack, "Scramjet Flameholder Ignition and Blowout Mapping", 69th JANNAF Propulsion Meeting / Programmatic and Industrial Base Meeting / 51st Combustion / 39th Airbreathing Propulsion / 39th Exhaust Plume & Signatures / 33rd Energetic Systems Hazards / 16th Modeling & Simulation Joint Subcommittee Meeting. 6-10 June. Newport News, VA. (2022)

[3] T. Bergman, A. Lavine, F. Incropera, D. Dewitt, *Introduction to Heat Transfer Sixth Edition*, Hoboken, NJ: John Wiley & Sons, 2011. [Textbook]. p. 381, eqn 6.7

[4] P. Gradl, C Protz, K. Cooper, C. Garcia, D. Ellis, L. Evans, "GRCop-42 Development and Hot-Fire Testing Using Additive Manufacturing Powder Bed Fusion for Channel-Cooled Combustion Chambers", *55th AIAA/SAE/ASEE Joint Propulsion Conference 2019,* (AIAA-2019-4228), 19-21 August. Indianapolis, Indiana. Doi: 20190030433, p. 4-7 (2019)

[5] H. de Groh III, D. Ellis, W. Loewenthal, *Comparison of GRCop-84 to Other Cu Alloys With High Thermal Conductivities,* p. 32, Feb. 2007, doi: 20070017311, NASA/TM-2007-214663

[6] T. Bergman, A. Lavine, F. Incropera, D. Dewitt, *Introduction to Heat Transfer Sixth Edition*, Hoboken, NJ: John Wiley & Sons, 2011. [Textbook]. p. 516, eqn 8.60

[7] S. Manson, G. Halford, "A Method of Estimating High Temperature Low Cycle Fatigue Behavior of Materials", *NASA Technical Memorandum,* Cleveland, Ohio. NASA TM X-52270. [Technical Paper Online] (1967)

[8] R. Baurle, J. White, T. Drozda and A. Norris, "VULCAN-CFD User Manual: Ver. 7.1.0," NASA Technical Report TM-2020-5000767, 2020.